

# A digital correlator upgrade for the Arcminute MicroKelvin Imager

Jack Hickish,<sup>1,2★</sup> Nima Razavi-Ghods,<sup>2★</sup> Yvette C. Perrott,<sup>2</sup> David J. Titterington,<sup>2</sup> Steve H. Carey,<sup>2</sup> Paul F. Scott,<sup>2</sup> Keith J. B. Grainge,<sup>3</sup> Anna M. M. Scaife,<sup>3</sup> Paul Alexander,<sup>2</sup> Richard D. E. Saunders,<sup>2,4</sup> Mike Crofts,<sup>2</sup> Kamran Javid,<sup>2</sup> Clare Rumsey,<sup>2</sup> Terry Z. Jin,<sup>2</sup> John A. Ely,<sup>2</sup> Clive Shaw,<sup>2</sup> Ian G. Northrop,<sup>2</sup> Guy Pooley,<sup>2</sup> Robert D’Alessandro,<sup>2</sup> Peter Doherty<sup>2</sup> and Greg P. Willatt<sup>2</sup>

<sup>1</sup>Radio Astronomy Laboratory, University of California, Berkeley, CA 94720, USA

<sup>2</sup>Astrophysics Group, Cavendish Laboratory, 19 J. J. Thomson Avenue, Cambridge CB3 0HE, UK

<sup>3</sup>Jodrell Bank Centre for Astrophysics, Alan Turing Building, School of Physics and Astronomy, University of Manchester, Oxford Road, Manchester, M13 9PL, UK

<sup>4</sup>The Kavli Institute for Cosmology, Cambridge, CB3 0HA, UK

Accepted 2018 January 4. Received 2017 December 22; in original form 2017 June 19

## ABSTRACT

The Arcminute Microkelvin Imager (AMI) telescopes located at the Mullard Radio Astronomy Observatory near Cambridge have been significantly enhanced by the implementation of a new digital correlator with 1.2 MHz spectral resolution. This system has replaced a 750-MHz resolution analogue lag-based correlator, and was designed to mitigate the effects of radio frequency interference, particularly that from geostationary satellites which are visible from the AMI site when observing at low declinations. The upgraded instrument consists of 18 ROACH2 Field Programmable Gate Array platforms used to implement a pair of real-time FX correlators – one for each of AMI’s two arrays. The new system separates the down-converted RF baseband signal from each AMI receiver into two sub-bands, each of which are filtered to a width of 2.3 GHz and digitized at 5-Gsps with 8 bits of precision. These digital data streams are filtered into 2048 frequency channels and cross-correlated using FPGA hardware, with a commercial 10 Gb Ethernet switch providing high-speed data interconnect. Images formed using data from the new digital correlator show over an order of magnitude improvement in dynamic range over the previous system. The ability to observe at low declinations has also been significantly improved.

**Key words:** instrumentation: interferometers – techniques: interferometric – telescopes.

## 1 INTRODUCTION

The Arcminute Microkelvin Imager (AMI) instrument consists of two synthesis radio telescopes located at the Mullard Radio Astronomy Observatory near Cambridge. AMI, which operates in the 12–18 GHz frequency band, was designed primarily for the study of galaxy clusters by observing secondary anisotropies in the cosmic microwave background (CMB) arising from the Sunyaev–Zel’dovich (SZ) effect (Sunyaev & Zeldovich 1970).

AMI is made up of two arrays: the Small Array (SA) and the Large Array (LA). The SA telescope comprises ten 3.7 m diameter paraboloid dishes in a compact configuration and is designed for observing structures on arcminute scales. The LA, which was created by reconfiguring the eight 12.8 m dishes of the Ryle Telescope

has an angular resolution of 0.5 arcmin and has approximately 10 times the flux-density sensitivity of the SA. The LA, observing concurrently with the SA, is used to measure the intensities of contaminating small-diameter radio sources.

The original AMI correlator (Zwart et al. 2008) was of an analogue ‘XF’ design, whereby the antenna signals were cross-correlated over a range of delays and then Fourier transformed into spectral channels. The original correlator recorded visibilities in eight frequency channels over AMI’s 12–18 GHz band, providing limited capability for recognizing and removing interfering signals as well as limited ability to mitigate chromatic aberration out to the edge of field of view. As a result, the sensitivity of the instrument was significantly reduced, particularly at low declinations, where interference from geostationary satellites could result in up to 90 per cent of the data being unusable. The XF system had a performance that was also limited by the path-length inaccuracies of analogue delay compensation and analogue correlation, which

\*E-mail: [jackh@berkeley.edu](mailto:jackh@berkeley.edu) (JH); [nima@mrao.cam.ac.uk](mailto:nima@mrao.cam.ac.uk) (NR-G)

resulted in direction-dependent systematic errors and poor dynamic range.

Starting in 2014, a project was undertaken to build a digital correlator for the telescope based on the second-generation Reconfigurable Open Architecture Computing Hardware board (ROACH2<sup>1</sup>), developed by the Collaboration for Astronomy Signal Processing and Electronics Research (CASPER<sup>2</sup>) and used extensively in radio-astronomy digital signal processing (DSP) applications (Hickish et al. 2016). ROACH2 is a powerful real-time signal processing platform based around a Xilinx Virtex 6 Field Programmable Gate Array (FPGA) which provides up to 80 Gbps of Ethernet-based I/O, and may be interfaced with a variety of analogue to digital converters (ADCs). The primary goal of the project was to equip AMI with a digital correlator providing over 100 times the frequency resolution of the original system with superior inter-channel rejection, allowing better frequency-confinement of interfering signals as well as overcoming some of the limitations of analogue lag correlator. The wide bandwidth of the AMI receiver required an optimized FPGA correlator design, capable of operating at the relatively high clock speed of 312.5 MHz, to be developed. This correlator, which comprises an independent instrument for each of the AMI arrays, uses 18 ROACH2 boards (10 for the SA, and 8 for the LA) to digitize, channelize and then cross-correlate analogue inputs from the antennas in the AMI arrays. Communication between boards in each AMI array is achieved using an industry-standard 10 Gb Ethernet (10 GbE) network, with an off-the-shelf switch providing interconnect. This so-called ‘Packetized Correlator’ architecture was pioneered by the CASPER group (Parsons et al. 2008; Hickish et al. 2016) and has been well proven at multiple radio-telescopes (Kocz et al. 2015; Foley et al. 2016; Nita et al. 2016; Primiani et al. 2016).

In this paper, we summarize the design of, and first commissioning results from the new AMI correlator. In Section 2, we describe the architecture of the system deployed, which comprises an overhauled analogue front-end and a new digital back-end. In Section 3, details of the implementation of the digital back-end are presented. The instrument’s control system and data reduction pipeline are outlined in Sections 4 and 5, respectively, with commissioning results from the new system given in Section 6.

## 2 ARCHITECTURE OVERVIEW

The AMI correlator upgrade continues to use the front-end systems developed in Zwart et al. (2008), with a new final IF stage and digital signal processing backend. A summary of the telescope specifications is given in Table 1.

### 2.1 Analogue front-end

The AMI front-end system consists of a feed assembly, first down-converting mixer and second mixer stage as shown in Fig. 1. Each feed assembly contains the horn antenna, cryostat, radio-frequency (RF) amplifiers, noise injection, bias box, and the cryogenic support system. Each cryostat has three temperature zones separated by thermal shielding: 15–20 K, 50–70 K, and 300 K. There are two RF amplifiers: the first is mounted on the 20 K coldhead of the cryostat, and the second is at 300 K. Noise at a constant level may be switched into the front-end via a noise source which is outside the cryostat on the SA, and inside the cryostat at 300 K on the LA. A detailed

**Table 1.** Summary of AMI technical data. Specifications pertaining to frequency coverage (slightly reduced) and frequency resolution (dramatically increased), which have changed since Zwart et al. (2008) appear in bold.

	Small array	Large array
Antenna diameter (m)	3.7	12.8
Antenna efficiency	0.75	0.67
Number of antennas	10	8
Number of baselines	45	28
Baseline lengths (m)	5–20	18–110
Primary beam (@15.5 GHz)	20′	5′
Synthesized beam	≈3′	≈30′′
Flux sensitivity (mJy s <sup>1/2</sup> )	30	3
Declination range (°)	>−15	>−20
Elevation limit (°)	+20	+5
<b>Observing frequency (GHz)</b>	13.1–17.9	
<b>Number of channels</b>	4096	
<b>Channel bandwidth (MHz)</b>	1.22	
System temperature (K)	25	
Polarization measurement	I+Q	

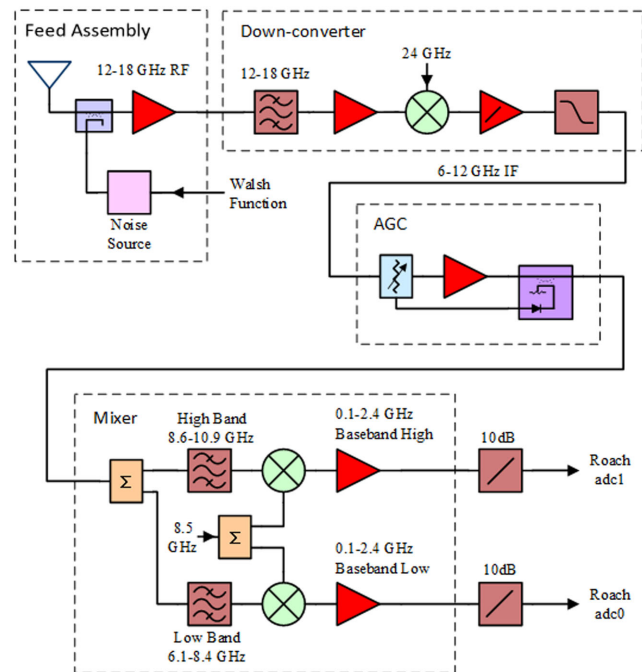


**Figure 1.** The AMI RF and IF system diagram. Isolators and attenuators used in the chain are not shown. The *Mixer* units in the system are newly developed as part of the correlator upgrade.

description of the feed assembly, down-converter, and Automatic Gain Control (AGC) systems, which have not been modified as part of this work, is given in Zwart et al. (2008).

The RF (12–18 GHz) signals from the antenna feeds are down-converted to an intermediate-frequency (IF) band of 6–12 GHz using a 24 GHz local oscillator (LO). Phase-switching is provided by modulating this LO signal by Walsh functions which are generated by the digital correlator. The IF is fed from the antenna hub to a correlator room where an AGC unit is used to maintain a constant power level prior to further downmixing.

A second mixer assembly splits the down-converted IF output into two 2.3 GHz wide sub-bands by first filtering the low and high bands and then mixing with an 8.5 GHz common local

<sup>1</sup> [https://casper.berkeley.edu/wiki/ROACH-2\\_Revision\\_2](https://casper.berkeley.edu/wiki/ROACH-2_Revision_2)

<sup>2</sup> <https://casper.berkeley.edu>

**Table 2.** The AMI frequency bands.

	RF (GHz)	IF (GHz)	Baseband (GHz)
Low Band	15.6–17.9	6.1–8.4	0.1–2.4
High Band	13.1–15.4	8.6–10.9	0.1–2.4

oscillator. Custom-manufactured low-pass filters are used to further limit the bandpass of the baseband signal prior to being fed into ADCs. The terms ‘low band’ and ‘high band’ used here to describe the two AMI correlator basebands refer to the frequencies of the mixer bandpass filters, not their respective RF input frequencies, as shown in Table 2. The second mixer assembly for the new system provides approximately 5 GHz of the original 6 GHz AMI frequency channel. The improvements in dynamic range are evident even with the loss in sensitivity due to processing less channel bandwidth.

## 2.2 Digital back-end

The AMI digital correlator is implemented using the standard ‘FX’ architecture favoured by most modern correlators. In this architecture, analogue signals from each antenna are first digitized before being split into spectral channels using an FFT-based algorithm (the ‘F’ processing stage). Spectra from pairs of antennas are then multiplied and time-averaged on a per-frequency-channel basis (the ‘X’ processing stage). The F-stage processing of such a correlator can be trivially parallelized over the multiple antennas in an array, whilst the X-stage computation is parallel over multiple frequency channels. Interconnect exists between the F and X processors to facilitate a data transpose – often referred to as a *corner-turn* – which allows data to be aggregated appropriately so as to allow parallel processing.

The AMI correlator uses FPGAs to perform the F and X processing, owing to their support for high input and output data rates and ease of interfacing to high-speed ADCs. Interconnect is provided by commercial off-the-shelf (COTS) 10 Gb s<sup>-1</sup> Ethernet (10 GbE) switches, which offer cost-effective, flexible, and reliable performance. Such switches also support useful functionality such as multicast (point to multi-point data transmission) which may be used in future correlator operating modes. This ‘packetized correlator’ architecture has been well developed by the CASPER collaboration, which provides and maintains software and firmware libraries to facilitate rapid deployment of digital astronomical systems.

Though not required by the packetized architecture, the AMI correlator design uses the same physical processors for its F and X stages (Fig. 2). This allows the complete system to be efficiently implemented with minimal hardware. Once correlation matrices have been computed and averaged for an appropriate time window, these are sent over a 1 Gb Ethernet network where the results are aggregated by a standard x86 GNU/Linux server.

### 2.2.1 Digital hardware

The digital processing platform chosen for the AMI correlator is the mature and ubiquitous CASPER-designed ROACH2 board<sup>3</sup>. This is a general-purpose FPGA platform, built around a Xilinx Virtex 6 (XC6VVSX475T-1FFG1759C) FPGA, supported by four 72 Mb QDR memory chips, 1 GB of DRAM, and up to eight 10 GbE interfaces via a pair of SFP+ mezzanine cards. The ROACH2

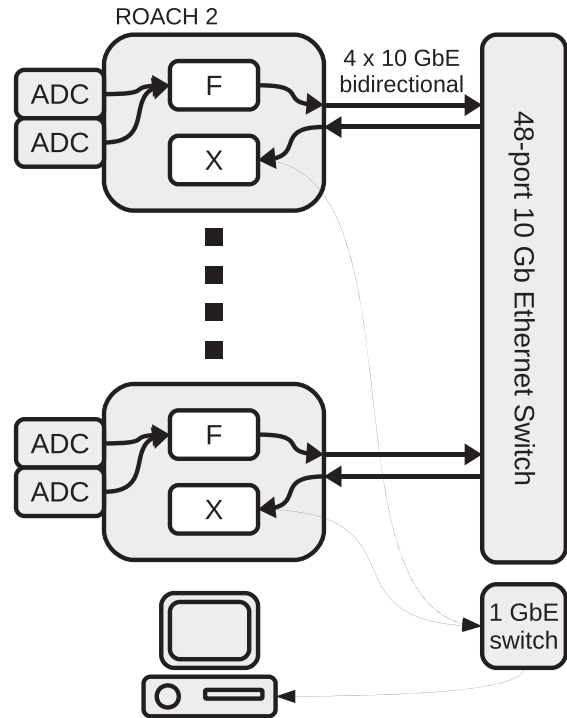


**Figure 2.** The top-level correlator architecture. Digitization is performed by a pair of 5 Gbps ADC cards interfaced to a ROACH2. The ROACH2 firmware implements both channelization and cross-multiplication functionality, with a 10 GbE switch providing interconnect between the two phases of processing. Averaged correlation results are output over a separate 1 Gb Ethernet network.

also provides two 40-pair LVDS interfaces via Z-DOK connectors, which can be used to interface the ROACH2’s FPGA to a variety of CASPER-supported ADC cards.

For the AMI correlator, both Z-DOKs are populated with CASPER ADC1x5000<sup>4</sup> cards. Each of these hosts an e2v EV8AQ160: a quad-core digital sampler capable of sampling a single RF input at up to 5 Gbps. The ADC1x5000 was designed by the Academia Sinica Institute of Astronomy and Astrophysics (ASIAA) and has been extensively characterized by Patel et al. (2014) as part of the development of a new wideband correlator for the Submillimetre Array (SMA, Primiani et al. 2016).

Each ROACH2 in the AMI system is fed with two timing signals derived from a COTS Trimble Thunderbolt E GPS-disciplined oscillator, which provides a pulse-per-second (PPS) reference and 10 MHz frequency standard. The PPS is distributed to each ROACH2 in the system via a 16-way buffered splitter and is used to synchronize and timestamp the data outputs from each board. The 10 MHz reference is used to derive a 2500 MHz clock, which is amplified and split so that it may drive the 5000 Msps ADC samplers synchronously.

The complete ROACH2 processing node is shown in Fig. 3. The node interfaces comprise:

- (i) An SMA input for a 2.5 GHz clock (used to derive the 5 Gbps ADC sampling rate).
- (ii) An SMA input for a TTL pulse-per-second (PPS) time reference.

<sup>3</sup> [https://casper.berkeley.edu/wiki/ROACH-2\\_Revision\\_2](https://casper.berkeley.edu/wiki/ROACH-2_Revision_2)

<sup>4</sup> <https://casper.berkeley.edu/wiki/ADC1x5000-8>

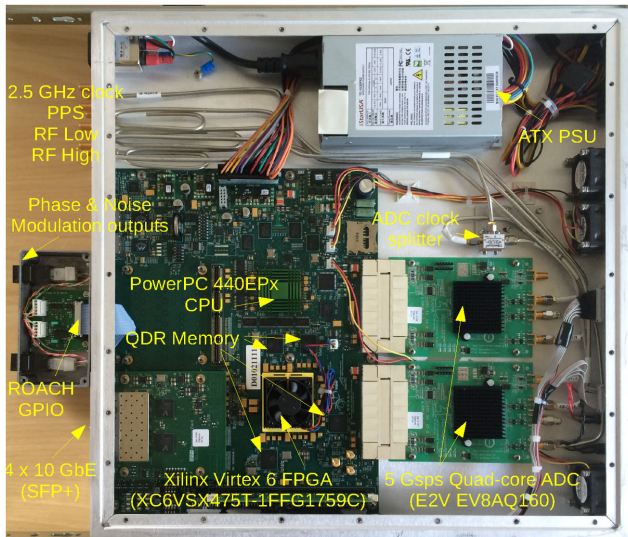


**Figure 3.** The CASPER ROACH2 platform on which the AMI digital correlator is implemented. Here, the board is shown with two 5 Gbps ADC daughter cards, a quad-SFP+ mezzanine card, and a Walsh switch interface box.

(iii) SMA inputs for the high- and low-baseband inputs from the analogue front-end of a single AMI antenna.

(iv) Level-shifting circuitry to allow interfacing of the ROACH2 FPGA with the AMI phase and noise modulation infrastructure (see Section 3.2).

(v) A 1000BASE-T Ethernet interface to the FPGA, for data output.

(vi) A 1000BASE-T Ethernet interface to ROACH2's on-board CPU, which is used for controlling and monitoring the board.

(vii) Four SFP+ connectors, each providing a 10 GbE interface.

A key part of the correlator hardware infrastructure is the 10 GbE switch facilitating interconnection between the 10 (8) boards in the SA (LA) system. This is a Mellanox SX1012, 12-port, 40 Gb Ethernet switch, capable of operating as a 48-port 10 GbE switch using interconnecting cables to connect each of the switch's QSFP+ ports to four independent SFP+ interfaces.

The complete rack of digital equipment for the SA correlator is shown in Fig. 4.

### 3 CORRELATOR FIRMWARE

#### 3.1 Analogue-to-digital converters

The CASPER collaboration (and in particular CASPER members in the Submillimetre Array correlator group) provide open-source interface firmware<sup>5</sup> and software<sup>6</sup> to stream data from the e2v EV8AQ160 ADC into the ROACH2 board via its Z-DOK connector. This interface expects data to be presented to the FPGA at a quarter of the ADC sample rate, over four parallel 8-bit buses. At a maximum sampling rate of 5 Gbps, this results in 32 parallel data lines, each running at 1.25 Gbps. Once captured by the FPGA, these parallel samples are demultiplexed by a further factor of four, so that on every FPGA clock cycle, 16 samples are processed in parallel. In the AMI design, the signal processing pipeline is clocked

<sup>5</sup> [https://github.com/casper-astro/mlib\\_devel](https://github.com/casper-astro/mlib_devel)

<sup>6</sup> [https://github.com/sma-wideband/adc\\_tests](https://github.com/sma-wideband/adc_tests)

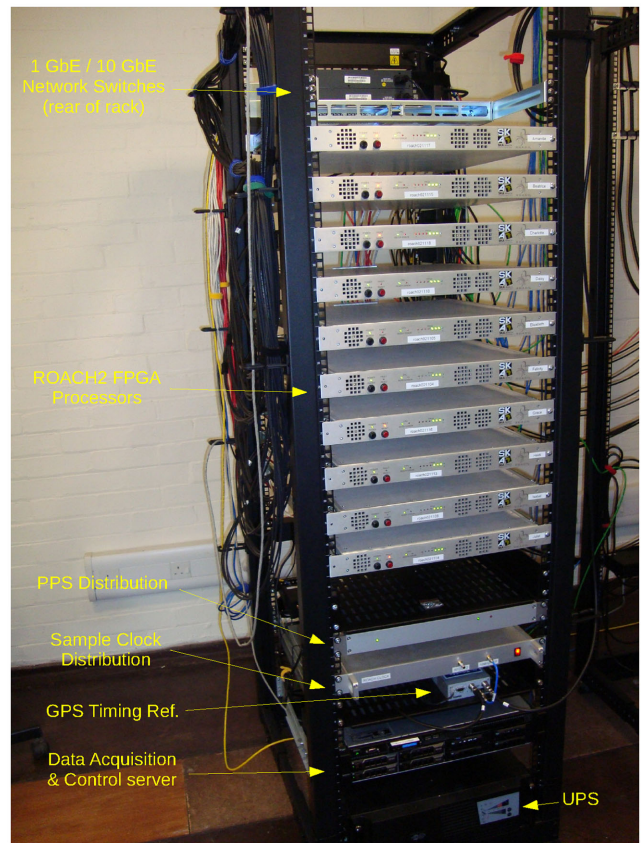


**Figure 4.** The digital correlator rack for the 10-antenna AMI SA.

synchronously with the ADC, at a rate of 312.5 MHz. At the time of design, the interface provided by CASPER did not function at the full 5 Gbps rate of which the ADCs are capable. As part of this work, the interface has been modified to increase performance and released back to the CASPER community. We note that since the ADC used by AMI is of multicore design, data are liable to artefacts caused by mismatch in the timing, gain, and voltage offsets of the different sampler cores Patel et al. (2014). Currently, the AMI system flags the frequency channels associated with artefacts from voltage offsets (this is the channel at the centre of the digitized band), but does not correct for timing and gain mismatches. Further work is needed to assess the effect of these mismatches on the broad-band images AMI produces, but they are not thought to limit the performance of the array, due to the suppression effects provided by fringe-tracking, and time-averaging, and frequency-averaging.

#### 3.2 Front-end noise injection and phase switching control

In the original AMI analogue correlator, phase and noise modulation functions were generated by a bank of look-up tables driven by a 65536 Hz counter. In order to simplify the new digital system, it was decided that the correlator FPGAs should be responsible for generation of the switching signals. In this way, the switching frequencies are synchronous with the ADC sampling, and can easily be chosen such that an integral number of switching periods occur in each channelization window and correlator integration period.

In order that the FPGAs are able to drive the existing front-end switching infrastructure, simple interface boards were constructed to convert a pair of 1.5 V ROACH2 general-purpose IO (GPIO) outputs to drive 5 V differential signals over Category 5 UTP cable.

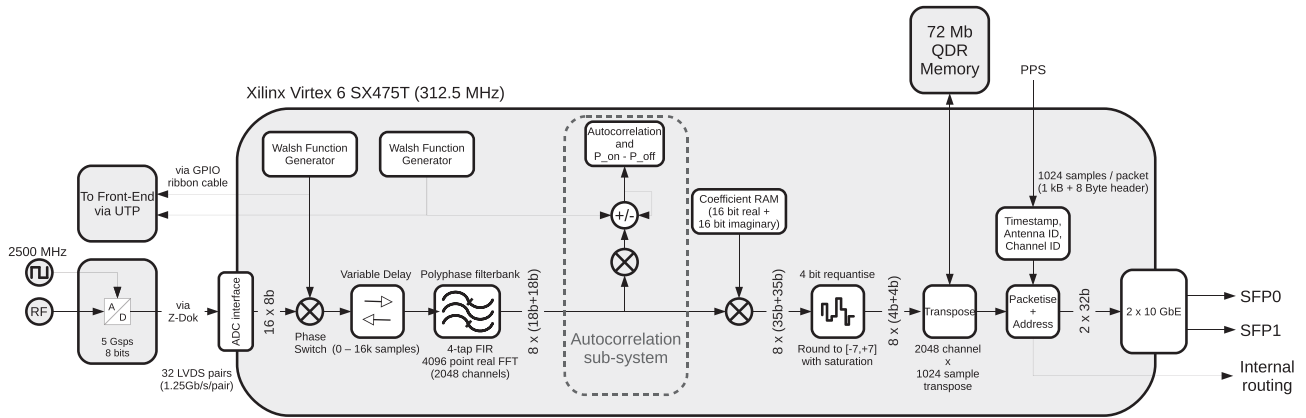


**Figure 5.** A schematic depiction of the AMI F-Engine firmware. Two such F-Engines are instantiated on each ROACH2 FPGA.

Though unused in the AMI correlator, the interface boards are also capable of converting a pair of differential signals to single-ended 1.5 V inputs, which may be used to drive ROACH2 GPIO pins.

### 3.3 F-engine

The bulk of the new AMI correlator design comprises the ‘F-engine’ processing pipeline; the channelization of pairs of 5 Gbps data streams into 2048 critically sampled subbands, which are output over 10 GbE as User Datagram Protocol (UDP) data streams (Fig. 5). Stages of the pipeline are:

#### 3.3.1 Phase-demodulation

Immediately after samples are captured into the FPGA, the phase modulation applied in the antenna’s first mixer stage is removed by a simple multiplication of ADC samples by  $\pm 1$ . The modulation/demodulation pattern used is unique to each antenna, and stored in the firmware in a runtime-programmable look-up table. A programmable delay between the modulation GPIO output (Section 3.2) and the internal demodulation signal allows compensation for delays associated with cable lengths of the control and RF signals.

#### 3.3.2 Coarse delay

After demodulation, each antenna’s digital data stream may be delayed by up to 16 384 ADC samples. This delay allows for compensation of geometric delays in the array (the largest baseline in the LA is approximately 110 m) and RF cabling. The desired delays are calculated by the telescope control computer based on the current pointing of the array, and any pre-computed delay calibration solutions. The frequency resolution of the AMI digital correlator is 1.22 MHz, giving an inverse-channel-bandwidth of around 800 ns. This inverse-bandwidth sets the accuracy with which variable delays must be applied to avoid losing coherence of the antenna signals; for AMI, it is sufficient to update coarse delays on approximately second time-scales. For simplicity of data analysis, the correlator control software ensures that delay updates are applied synchronously with new visibility accumulations, such that no coarse delay changes occur mid-integration.

#### 3.3.3 Polyphase filterbank

The largest component of the F-Engine processing pipeline is a polyphase filterbank (originally proposed by Bellanger et al. 1976, see Harris & Haines 2011; Price 2016 for relevant overviews), which breaks the 5 Gbps data streams into 2048 critically sampled subbands, each of bandwidth 1.22 MHz. The CASPER group provide parametrized finite impulse response (FIR) filter and fast Fourier transform (FFT) libraries for implementing polyphase filterbanks – these have been utilized here, after various optimizations were applied to reduce FPGA resource utilization and to maximize clock frequency. These optimizations are publically available<sup>7</sup> and include:

- (i) Reductions in overall FPGA fabric use by reducing control logic.
- (ii) Improved timing performance of reordering blocks when per-clock enabling is not necessary.
- (iii) Utilization of FPGA single instruction, multiple data (SIMD) instructions for complex addition and subtraction operations.
- (iv) Improved timing performance of integer rounding operations by allowing the use of dedicated FPGA arithmetic cells.

Signals within the channelizer are processed with 18 bits of precision in both channelizer coefficients and data path, resulting in output subbands (spectra) which are complex-valued, with each of the real and imaginary components represented as signed 18-bit numbers.

#### 3.3.4 Autocorrelation sub-system

After channelization, the power of each spectrum is computed and fed into a vector accumulator. This provides (without requiring the downstream correlator infrastructure) an averaged power-spectrum for each antenna signal. The autocorrelation subsystem can also demodulate by the Walsh pattern used to drive the noise injection at each of the antenna feeds, providing a measurement of the system temperature of each antenna. Since the system temperature of antennas varies with weather, constant measurements of these ‘rain-gauge’ values are performed and stored with final data products.

<sup>7</sup> See the `ami_devel` branch of the CASPER libraries at [https://github.com/jack-h/mlib\\_devel/tree/ami-devel](https://github.com/jack-h/mlib_devel/tree/ami-devel).

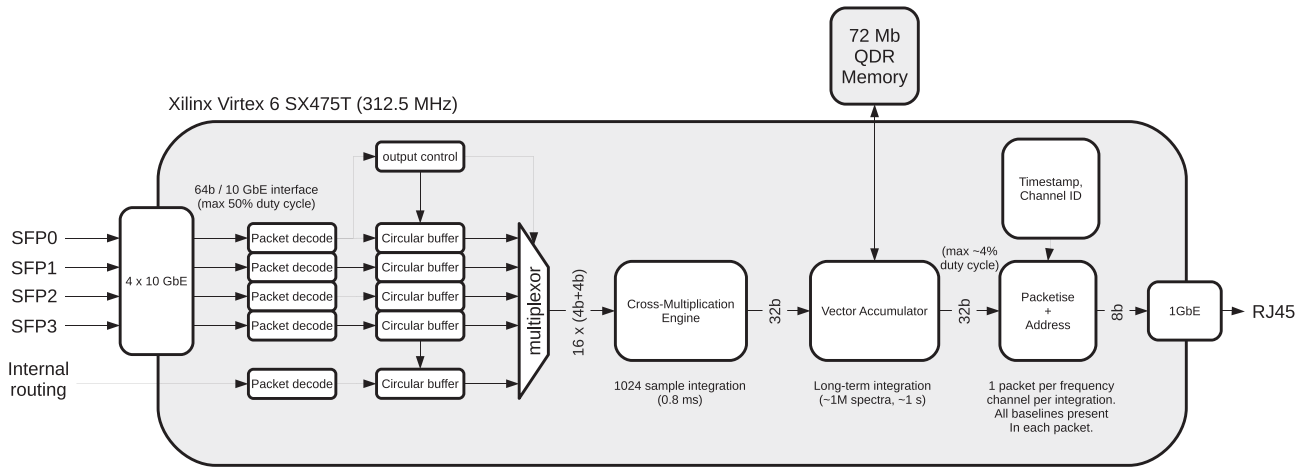


**Figure 6.** A schematic depiction of the AMI X-Engine firmware.

### 3.3.5 Requantization

In order to reduce FPGA output bandwidth, data samples are rounded to 4-bit values – real and imaginary parts in the range  $(-7, +7)$  – with saturation logic prior to being streamed over Ethernet. In order to use the available 4-bits of range most efficiently, before quantization each of the 2048 subbands associated with an ADC data stream are equalised by multiplying by per-antenna, per-subband coefficients. These coefficients are runtime-programmable, and can be calculated by examining data either from the autocorrelation sub-system or the final correlator data products.

### 3.3.6 Data buffering and transmission

The CASPER cross-correlation module used in the correlator (Parsons et al. 2008; Hickish 2014) expects data to be presented in windows of 1024 samples from each frequency channel in turn. To achieve this, 1024 spectra, each of 2048 channels, must be re-ordered in memory to gather similar channels into contiguous blocks. This reordering operation requires a buffer of  $\sim$ MB size. Such memory is not available on the FPGA chip itself, so external 72 Mb Quad Data Rate (QDR) memory chips (of which four are provided by the ROACH2 platform) are used for this reorder operation.

Once data are suitably ordered, they are transmitted as streams of UDP packets over an Ethernet network. The destination address of each packet is determined by the frequency channel associated with the data in that packet’s payload, with the end result that each ROACH2 in the network receives data associated with all antennas in the array, but only certain frequency channels.

## 3.4 Data interconnect

After 4-bit requantization, the data output rate from each dual-band F-engine is 40 Gbps. These data are transmitted as a stream of UDP packets, with each packet’s payload comprising 1024 time samples from a single frequency channel. When transmitted over Ethernet as a stream of UDP packets, transmission protocol overhead – Ethernet, internet protocol, UDP, and application headers – must also be accommodated. In order to transmit the stream over four 10 GbE links, the AMI system takes advantage of the fact that F- and X-processors are located on the same physical hardware. This allows frequency channels with the same source and destination ROACH2

to be routed internally, bypassing the Ethernet interconnect. Such routing reduces the necessary throughput of the interconnection by 10 per cent (12.5 per cent) for the Small (Large) AMI array. Including transmission protocol overhead, the aggregate output data rate from each 10 GbE interface is 9.4 (9.1) Gbps for the Small (Large) array. The full 2.5 GHz digitized bands are output, though in the case of the SA only 2040 of the total 2048 frequency channels from each band are processed, in order to equally share channels among the 10 processing nodes in the system.

## 3.5 X-engine

The second stage in the correlator is the ‘X-engine’, which is responsible for performing a per-frequency-channel cross-multiplication of data from different antenna pairs. The X-engine pipeline is shown in Fig. 6, and its components comprise:

### 3.5.1 Input buffering

Data are received from the Ethernet network on the same four SFP+ interfaces used for transmission, as well as an internal routing path. The order that packets from different antenna sources are received from the network is not known in advance – a circular buffer is used to collect, and appropriately order, data from different antennas prior to cross-multiplication. Once all antenna packets have been received for a given frequency channel,  $n$ , which is indicated by the arrival of a packet of channel  $n + 2$ , a window of data is streamed into a cross-multiplication engine.

### 3.5.2 Cross-multiplication

The cross-multiplication engine is responsible for taking 1024 samples from a single frequency channel from all antennas, and delivering a visibility matrix integrated over these samples. The correlation engine used in AMI is based on a ‘windowed X-engine’ design by Parsons et al. (2008) which is now maintained by the CASPER community. The AMI version of this module has been ported to Verilog (rather than the CASPER standard of Xilinx System Generator and MATLAB Simulink). This makes the module more portable to non-CASPER projects which do not use Simulink and more easily version controlled and simulated using industry-standard tools which are not designed for use with Simulink model files. As part

**Table 3.** FPGA resource utilization in the AMI SA correlator design. The AMI LA design uses slightly fewer resources, owing to the smaller number of antennas requiring correlation in the X-engine stage of the design.

	DSP slices	BRAMs (36 kB)	LUTs	Flip flops
Coarse delay (dual-band)	0	16	2024	2314
FIR filter (dual-band)	128	66	3952	11 890
FFT (dual-band)	736	112	38 206	100 748
X-engine input buffers	0	81	3162	10 747
X-engine	98	18	2002	4722
Total design	1203	409	105 068	166 051
FPGA capacity	2016	1064	297 600	595 200
Per cent utilization	60	38	35	28

of the porting process, the module was also significantly optimized to minimize FPGA resource utilization and maximize performance.

First, AMI’s X-engine has a parameterisable input bandwidth, which can be any multiple of the FPGA clock speed. This allows a reduction in control-logic versus multiple instances of a fixed input-bandwidth engine. Secondly, the cross-multiplication and accumulation cores at the heart of the X-engine have been optimized for 4+4-bit complex inputs, allowing a 75 per cent reduction in multiplier use. This is achieved by offsetting the 4-bit correlator inputs to unsigned values, and appropriately packing pairs of them in 18-bit representations such that four 4-bit multiplications may be computed in a single  $18 \times 18$ -bit operation. A full description of this implementation can be found in Hickish (2014), which builds on the 4-bit packing speed-ups of de Souza et al. (2007) and is similar to more recent work targeting cross-multiplication of astronomical signals on Graphics Processing Units (GPUs) by Klages et al. (2015). As a result, the footprint of the cross-multiplication component of the AMI digital correlator has been reduced to a very small fraction of the overall design (Table 3). The code for this X-Engine is freely available<sup>8</sup> and is provided with a parametrized Simulink wrapper for use in CASPER systems. Though not used in the AMI project, a dual-polarization version of this module is under development, which provides a drop-in replacement for the standard CASPER Simulink module and offers a superset of the CASPER block’s parameters.

### 3.5.3 Vector accumulator

Per-frequency-channel visibility matrices, which have been integrated over 1024 samples, must be further time-averaged to reduce output data-rate to an acceptable level. This long-term (approximately second) averaging uses external Quad Data Rate (QDR) memory for data storage, at the end of which data are transmitted via a 1 Gb Ethernet interface to a data acquisition and storage server.

## 3.6 FPGA floorplanning

A significant hurdle in the deployment of the new AMI correlator was achieving timing-closure of the firmware designs at the required 312.5 MHz FPGA clock rate. Ultimately, this was achieved by constraining the placement of most of the  $\sim 1000$  multiplier cores and  $\sim 400$  RAM blocks in the design to small regions of the FPGA chip. Placement was manually defined for most modules, but in the case

of the FFT cores, a pair of which comprise the majority of the signal processing in the firmware, a set of PYTHON scripts was used to automate constraint generation. These scripts compute the number of multiplier and memory cores needed by each FFT, based on the known number of DSP slices and memory blocks needed by the CASPER FFT butterfly architecture, and the number of butterflies required to implement an FFT meeting the bandwidth and transform length specifications of the AMI channelizer. Constraints are then generated which stripe sequential butterflies over user-defined columns of DSP and memory resources. Having placed these resources, much of the FFT logic, which aims to provide pipelining between arithmetic components, could be removed, resulting in an FFT circuit that is smaller, can be run at higher clock rate, and, critically, has timing performance which is relatively stable when other areas of the FPGA design are modified. To the knowledge of the authors, the AMI design represents the fastest clocked ROACH2 in any deployed packetized-correlator system, with the largest instantaneous processed bandwidth per board. We note, however, that the AMI firmware resource requirements (Table 3) are modest when compared to some other deployments, such as Primiani et al. (2016). Experience with newer FPGA platforms also suggests that many of the timing issues encountered during development of the AMI correlator may be unique to the ROACH2’s Virtex 6 FPGA.

## 4 CONTROL SYSTEM

The control systems for the two arrays are independent, and are described in detail in Zwart et al. (2008). In each case, the only modifications needed for the new correlator have been replacement of the correlator microprocessor by the data acquisition and control server, situated in the digital rack and visible in Fig. 4, and replacement of the Sun-Microsystems workstation used for telescope and observation control by a Linux desktop system. Apart from the data acquisition components described below, the rest of the control software, written in C for the Solaris operating system, has simply been recompiled for the Linux platform.

### 4.1 Data acquisition

The Linux server used for correlator control and data acquisition is a standard single-socket machine, configured with 20 TB of local disc storage to accommodate several months of raw data. Data are captured from the ROACH2 boards over a 1 Gbps Ethernet interface (Fig. 2). A separate 1 Gbps interface is used for exchanging quick-look data samples and observation metadata with the telescope control system over a local Ethernet connection, as described in Section 4.2. This machine also acts as the DHCP/NFS server for the ROACH2 private network.

<sup>8</sup>See the `ami_devel` branch of the CASPER libraries at [https://github.com/jack-h/mlib\\_devel/tree/ami-devel](https://github.com/jack-h/mlib_devel/tree/ami-devel).

**Table 4.** Typical AMI data rates.

	Small array	Large array
Sampling rate (Mbps)	16.8	11.0
Recording rate (GBph)	8	5.2
8-h observation (GB)	64	42

A suite of PYTHON scripts to configure the ROACH2 boards and perform data collection has been developed for AMI, and is available on github<sup>9</sup>. There are separate scripts for programming and initialising the ROACH2 boards, and for computing the equalization coefficients for requantization (Section 3.3). Acquisition scripts deal with applying coarse path compensation delays to the digital data streams, exchanging metadata and visibilities with the telescope control machine and recording visibility data from the correlator at a programmable dump rate (currently every 0.86 s) in HDF5<sup>10</sup> format on the server's local discs. The arrangement for monitoring the relative system temperature of each antenna using amplitude-modulated injected noise referred to earlier and described in Zwart et al. (2008) is retained, and samples of the demodulated noise, derived from the autocorrelation measurements, are stored with the data for use during calibration processing.

Important features of the software design include the use of a standard configuration file, which allows the same code to be used for both arrays, and a Remote Dictionary Service (Redis<sup>11</sup>) key-value data store to share all data among the independently executed processes. A comprehensive set of utilities for monitoring the state of the correlator and visualizing the data sets is also included in the AMI software package.

Independently of data acquisition from the correlator, but at a similar sampling rate, metadata such as antenna pointing and instrumental monitoring information (e.g. cryostat temperatures, AGC readings) are collected by the telescope control machine, and exchanged with the correlator server over the local Ethernet.

## 4.2 Data handling

The HDF5 format data files, one per observation, include correlated visibility data, noise-injection measurements and metadata samples, and accumulate on discs local to the correlator control server. Typical raw data rates are shown in Table 4. These files are the primary data products from the telescope and contain uncalibrated, full spectral resolution data.

After each observation the HDF5 data set is converted to FITS-IDI<sup>12</sup> format for calibration and further processing using standard reduction packages, and is transferred from the observatory to a data repository at the Cavendish Laboratory. The conversion script is based on the pyFitsidi<sup>13</sup> PYTHON module, and also performs the following operations:

- (i) Removal of spike artefacts in a few fixed channels of the ADC readout which are contaminated by ADC core offset mismatches, by flagging these channels to zero.
- (ii) Removal of the channel readout delay phase shift.
- (iii) Re-ordering of the ADC channels into increasing RF order.

(iv) Fringe rotation to remove the astronomical path difference over each sub-band.

(v) Amplitude correction to compensate for loss-of-signal due to averaging over 0.86 s time windows; this is a function of the fringe rate and can be as much as a few per cent for some of the LA baselines.

(vi) Amplitude calibration for system temperature using the noise-injection system.

(vii) Flagging for instrumental problems (e.g. AGCs, cryostats, pointing, shadowing).

(viii) Optional binning of frequency channels, to reduce the data set size.

In parallel to the above, the raw data samples received from the correlator are binned to  $8 \times 0.625$  GHz frequency channels by a new task added to the real-time software on the telescope control system, and are recorded in legacy format for quick-look using the in-house software tool, REDUCE. These eight channels are chosen to correspond to those used by the old analogue correlator, and availability of these data sets has proved invaluable for data evaluation and diagnostics throughout the development process and during routine operation.

## 5 DATA REDUCTION

The FITS-IDI files contain visibility data to which instrumental flagging and some initial calibration steps have been applied, and these can now be imported to the standard reduction packages for radio interferometric data such as AIPS<sup>14</sup> and CASA<sup>15</sup> for full calibration, radio-frequency interference (RFI) flagging and map-making. A generalized pipeline script has been developed to process these data sets within the CASA framework, and deals with:

- (i) RFI flagging, both broad-band and at full frequency channel resolution.
- (ii) Bandpass (amplitude and phase) and flux calibration, using observations of standard calibrators.
- (iii) Phase calibration, using data from interleaved visits to nearby high flux density, unresolved radio sources.
- (iv) Imaging.

Primary beam correction and mosaicking is currently done in AIPS due to difficulties in importing new primary beam models into CASA.

This is the recommended route for processing AMI data for science. The eight-channel legacy format data sets described above are also available and can be processed using the in-house REDUCE software to provide useful results for some projects, but lose the benefits of the full spectral resolution that the new correlator provides.

## 6 COMMISSIONING RESULTS

### 6.1 RFIrejection

One of the main motivators for constructing a correlator with such improved spectral resolution was to be able to identify and remove RFI, which is typically confined to narrow frequency bands. RFI is generally worse at low elevation, due to the location of geostationary satellites. With the old correlator, this limited the useable declination

<sup>9</sup> [https://github.com/jack-h/ami\\_correlator\\_sw.git](https://github.com/jack-h/ami_correlator_sw.git)

<sup>10</sup> <https://www.hdfgroup.org/HDF5/>

<sup>11</sup> <http://redis.io/>

<sup>12</sup> <http://www.nrao.edu/aips/FITSIDI.pdf>

<sup>13</sup> <http://telegraphic.github.io/pyfitsidi>

<sup>14</sup> <http://www.aips.nrao.edu/>

<sup>15</sup> <http://casa.nrao.edu>

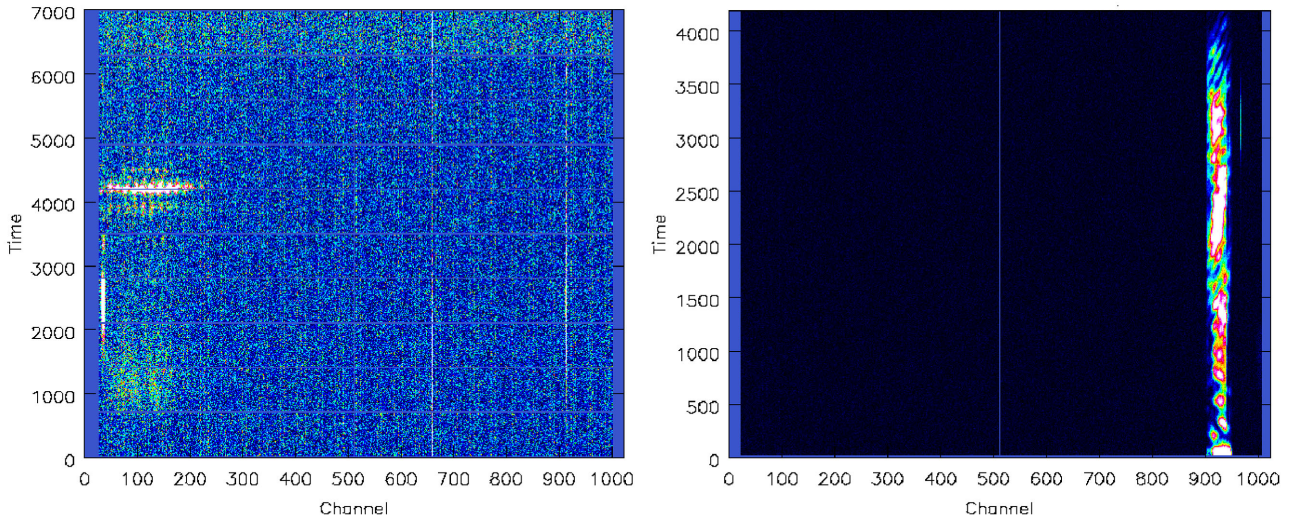


**Figure 7.** ‘Waterfall’ plots of a low-declination ( $\approx 0^\circ$ ) field observed with the LA (SA) on the left (right), showing time against channel for the lower (upper) half of the bandwidth on a single baseline. The RFI can be clearly seen as bright signals localized in frequency and time and is easily removed using automated algorithms such as ‘rflag’ in CASA; see Fig. 8.

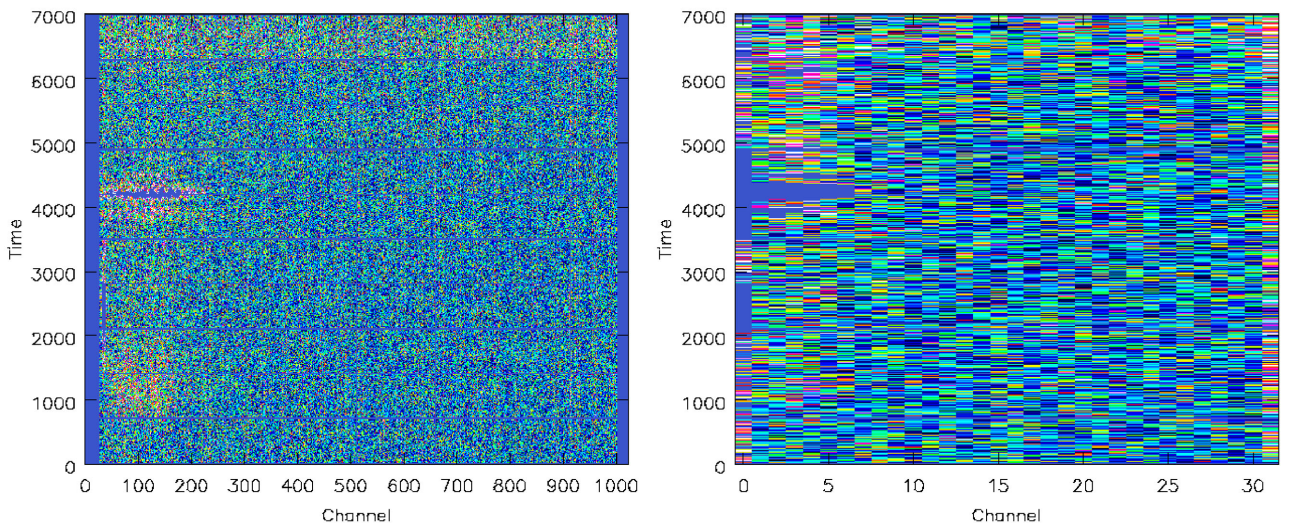


**Figure 8.** An illustration of RFI removal from the LA observation shown in Fig. 7. The left-hand side shows the effect of a  $5\sigma$  flagging step using the CASA ‘rflag’ algorithm; the bright, narrow-band signals have been removed as well as some of the wider-band signals. On the right, we have binned in frequency down to 32 channels and made another  $5\sigma$  cut, which removes most of the remaining wider-band signals.

range, particularly for the SA with its larger primary beam. RFI flagging levels on the SA reached  $\approx 85$  per cent at  $\delta \approx 2^\circ$ ; in practice observations were rarely made below  $\delta = 20^\circ$ . In Fig. 7, we show part of an observation of a low-declination ( $\approx 0^\circ$ ) field on both the LA and the SA with the new correlator. The RFI is clearly localized in time-space and frequency-space and affected regions of data can be easily excised using automated algorithms such as ‘rflag’ as implemented in CASA, which searches for deviations from the median r.m.s. of the data in time and frequency space; see the AIPS cookbook, section E.5<sup>16</sup> for more detail on the algorithm. This removal process is illustrated in Fig. 8. At  $\delta \approx 0^\circ$  the RFI flagging level is now  $\approx 20$  per cent on the LA and  $\approx 25$ – $35$  per cent on the SA. These are comparable to flagging percentages in similar frequency bands at other facilities, for example the Very Large Array

which loses  $\approx 15$  per cent at Ku-band<sup>17</sup>, accounting for the fact that the AMI arrays are more compact and therefore more sensitive to ground-based RFI, and have larger primary beams.

## 6.2 Dynamic range

The uneven lag spacings of the old correlator limited the dynamic range, since maps of fields near high flux density sources would be contaminated by artefacts introduced by the correlator. The digital correlator has removed this issue and consequently the dynamic range of the telescope, defined as the ratio of the brightest believable flux to brightest non-believable flux on the map, has increased from  $\sim 100$  to  $\sim 1000$ . Figs 9 and 10 show example maps of a bright

<sup>16</sup> <ftp://ftp.aoc.nrao.edu/pub/software/aips/TEXT/PUBL/COOKE.PS.gz>

<sup>17</sup> see e.g. [https://science.nrao.edu/facilities/vla/observing/RFI/jul-2014-d-configuration/Ku-Band\\_spectra\\_201407D](https://science.nrao.edu/facilities/vla/observing/RFI/jul-2014-d-configuration/Ku-Band_spectra_201407D)

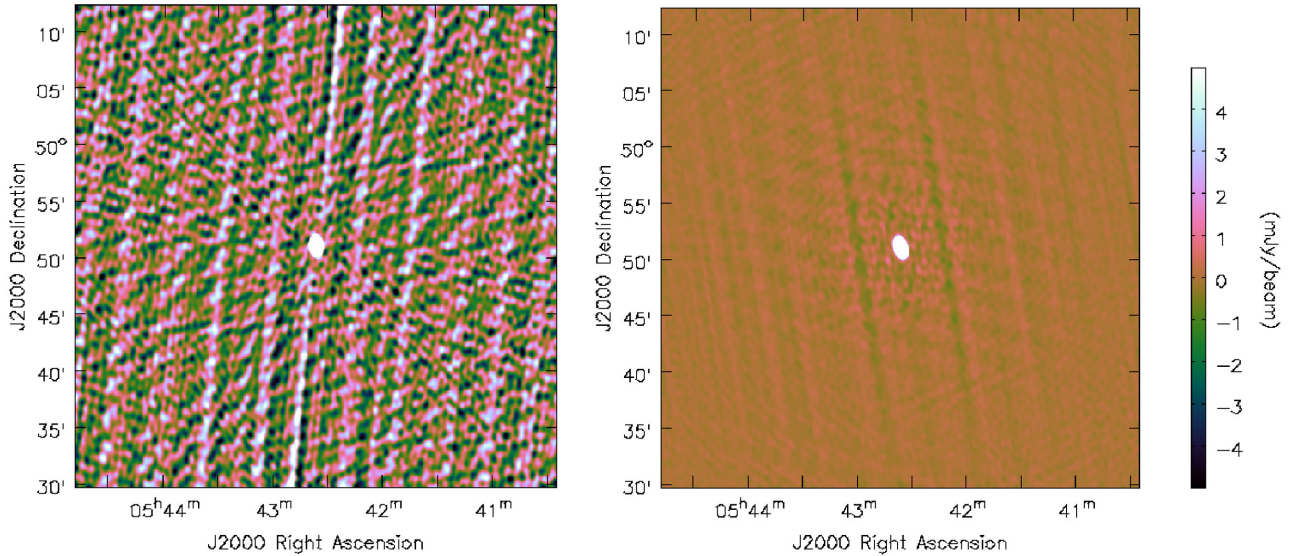


**Figure 9.** An LA observation of the bright, unresolved source 3C147 using the old (new) correlator on the left (right). The colour scales are the same, and have been truncated to show the systematic residuals around the source. These are at most 9.3 (1.1)  $\text{mJy beam}^{-1}$ , giving a dynamic range of 260 (2300).

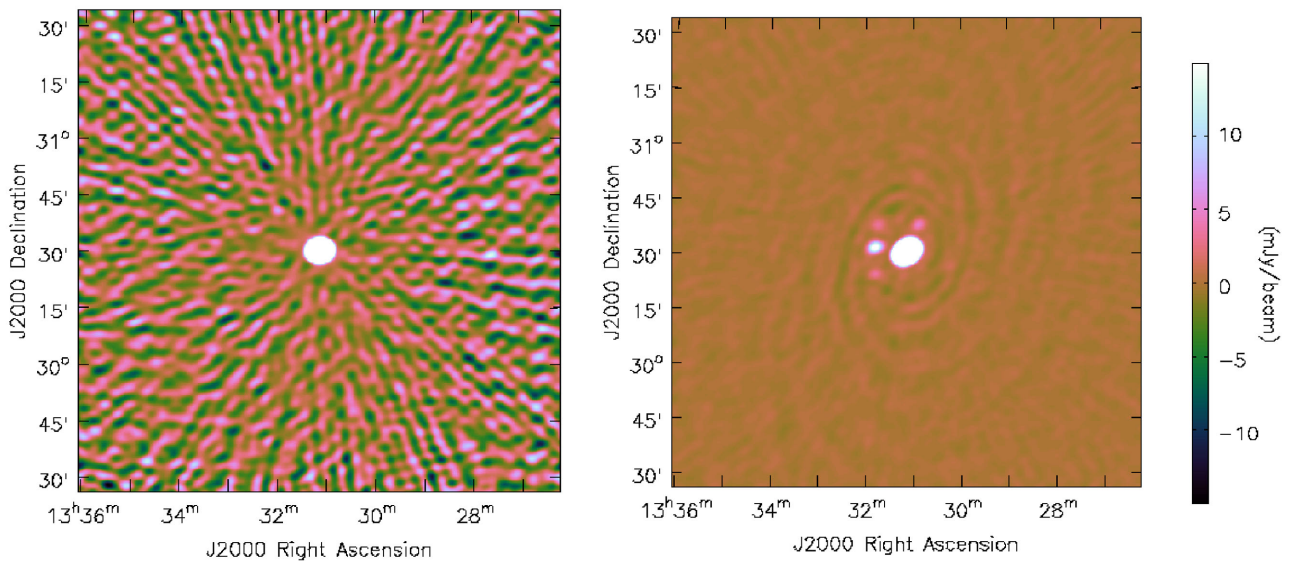


**Figure 10.** An SA observation of the bright, unresolved source 3C286 using the old (new) correlator on the left (right). The colour scales are the same, and have been truncated to show the systematic residuals around the source. These are at most 15 (1.2)  $\text{mJy beam}^{-1}$ , giving a dynamic range of 230 (3000). The integration time for the new correlator map was much longer, in order for the thermal noise to fall below the level of the systematic errors. The triple of sources visible to the east of 3C286 in the new correlator map is real (the central source is FIRST J133148.5+303147); the source to the north of 3C286 is also real (FIRST J133052.9+303807). They are all under the level of the residuals in the old correlator map.

source produced on the LA and the SA, in comparison to similar maps using old correlator data. The improved dynamic range of the new AMI system is enabling, for example, the observation of galaxy clusters containing bright radio galaxies, which were previously excluded from cluster samples potentially introducing unquantifiable biases.

### 6.3 Scientific collaboration

AMI has been operating routinely with the upgraded correlator since 2016 January. The telescope operates under the terms of a Scientific Collaboration Agreement involving the University of Cambridge and the University of Manchester, but welcomes external collabo-

rators. The current scientific programmes include: SZ observations of galaxy clusters, for example extending the previous follow-up of *Planck* galaxy clusters (Perrott et al. 2015); source surveys, extending the 10C source counts (e.g. Whittam et al. 2016) to lower flux densities and adding to the multiwavelength legacy data sets available in fields such as Stripe 82 (e.g. Ivezić et al. 2007 and COSMOS (e.g. Scoville et al. 2007); monitoring of variable and transient radio sources such as supernovae, GRBs, quasars, and X-ray binaries; observations of supernova remnants with reported anomalous microwave emission detections at low resolution (Génova-Santos et al. 2017, Onić, Urošević & Leahy 2017), to test for the presence of AME at the angular scales measured by AMI. In each case, the new correlator has allowed AMI to operate more effectively in

challenging radio source environments than was previously possible. This is a result of the greater RFI containment – which allows observations of low-declination fields – and enhanced dynamic range – which allows significant improvements in source subtraction capability – of the new instrument.

The first results using data taken with the upgraded correlator have been published (Mooley et al. 2017; Muñoz-Darias et al. 2017), with some work leveraging the new instrument in reobservations of sources originally detected by AMI’s analogue correlator (Perrott et al. 2018). More results are currently in preparation.

## 7 CONCLUSIONS

In this paper, we have presented a new digital correlator system for the AMI telescope, which replaces the telescope’s previous analogue lag-correlator. This real-time FX correlator is implemented using the popular ‘packetized correlator’ architecture, in which interconnect between processors is provided by commercial Ethernet switches. Processing in the new correlator is performed on CASPER open-source hardware; FPGA-based ROACH2 platforms are used to digitize, filter into 1.2 MHz-wide channels, and correlate a pair of down-converted sub-band signals at 5 Gsps, providing a usable RF band of 13.1–17.9 GHz. This wideband performance has been achieved by clocking the signal processing pipelines on the ROACH2’s Xilinx Virtex 6 FPGAs at 312.5 MHz, requiring optimization and floorplanning of the firmware design.

The improvement in performance of the new instrument when compared to the original analogue XF correlator is evident; the new correlator achieves over an order of magnitude improvement in imaging dynamic range, and is far more effective at operating in the presence of RFI – particularly interference at low-declination observations from geostationary satellites – owing to superior spectral resolution. As a result of the improved performance, a new scientific collaboration has been established for the operation of AMI, and a broad range of observations are currently being performed with the telescope, which is now highly subscribed.

## ACKNOWLEDGEMENTS

We acknowledge support from the European Research Council under grant European Research Council-2012- StG-307215 LODESTONE. The images in Figs 7–10 were prepared using the cubehe-

lix colour palette (Green 2011). This work has been supported by the generous donation of FPGA hardware and programming tools by the Xilinx University Program.

## REFERENCES

- Bellanger M., Bonnerot G., Coudreuse M., 1976, *IEEE Trans. Acoust. Speech Signal Process.*, 24, 109
- de Souza L., Buntun J., Campbell-Wilson D., Cappallo R., Kincaid B., 2007, in Bertels K., Najjar W., van Genderen A., Vassiliadis S., eds, *International Conference on Field Programmable Logic and Applications*. IEEE, Amsterdam, NL, p. 62,
- Foley A. R. et al., 2016, *MNRAS*, 460, 1664
- Génova-Santos R. et al., 2017, *MNRAS*, 464, 4107
- Green D. A., 2011, *Bull. Astron. Soc. India*, 39, 289
- Harris C., Haines K., 2011, *Publ. Astron. Soc. Aust.*, 28, 317
- Hickish J., 2014, PhD thesis, Uni. Oxford
- Hickish J. et al., 2016, *J. Astron. Instrum.*, 5, 1641001-12
- Ivezić Ž. et al., 2007, *AJ*, 134, 973
- Klages P., Bandura K., Denman N., Reclik A., Sievers J., Vanderlinde K., 2015, *IEEE 26th International Conference on Application-specific Systems, Architectures and Processors (ASAP)*, IEEE Toronto, ON, p. 164
- Kocz J. et al., 2015, *J. Astron. Instrum.*, 04, 1550003
- Mooley K. P. et al., 2017, *MNRAS*, 467, L31
- Muñoz-Darias T. et al., 2017, *MNRAS*, 465, L124
- Nita G., Hickish J., MacMahon D., Gary D., 2016, *JAI*
- Onić D., Urošević D., Leahy D., 2017, *AJ*, 153, 32
- Parsons A. et al., 2008, *PASP*, 120, pp. 1207
- Patel N. A., Wilson R. W., Primiani R., Weintraub J., Test J., Young K., 2014, *J. Astron. Instrum.*, 03, 1450001
- Perrott Y. C. et al., 2018, *MNRAS*, 473, 1157
- Price D. C., 2016, preprint ([arXiv:1607.03579](https://arxiv.org/abs/1607.03579))
- Primiani R. et al., 2016, *J. Astron. Instrum.*, 5, 1641006-810
- Scoville N. et al., 2007, *ApJS*, 172, 1
- Sunyaev R. A., Zeldovich Y. B., 1970, *Ap&SS*, 7, 3
- Whittam I. H., Riley J. M., Green D. A., Davies M. L., Franzen T. M. O., Rumsey C., Schammel M. P., Waldram E. M., 2016, *MNRAS*, 457, 1496
- Zwart J. T. L. et al., 2008, *MNRAS*, 391, 1545

This paper has been typeset from a  $\text{\TeX}/\text{\LaTeX}$  file prepared by the author.